IOP Publishing Nanotechnology
Nanotechnology 32 (2021) 195706 (15pp) https://doi.org/10.1088/1361-6528/abe3b3

Photocatalytic activity and photoelectrochemical properties of Ag/ZnO core/shell nanorods under low-intensity white light irradiation

M J Kadhim[1,*], M A Mahdi[1], J J Hassan[1] and Ahmed S Al-Asadi[2]

[1] Department of Physics, College of Science, University of Basrah, Basrah, Iraq
[2] Department of Physics, College of Education for Pure Science, University of Basrah, Iraq

E-mail: marooj2013@gmail.com

Received 29 September 2020, revised 26 January 2021
Accepted for publication 5 February 2021
Published 19 February 2021

Abstract

Zinc oxide (ZnO) nanorod thin films were prepared by CBD onto glass and FTO/glass substrates. Silver (Ag) nanoparticles were synthesized on the surface of the prepared ZnO nanorod thin films using electrochemical methods. The scanning electron microscopy images of the Ag/ZnO/glass core/shell nanostructure confirmed that the average particles size is 20 nm while it was 41 nm for Ag NPs that synthesized onto ZnO/FTO NRs. The photocatalytic activity of the prepared Ag/ZnO core/shell nanostructure was studied by analyzing the degradation of methylene blue (MB) dye under visible light. Various pH values (6 and 10) and exposure time (30–240) min were controlled to investigate the photocatalytic activity of as-prepared Ag/ZnO core/shell nanostructure and that annealed at 200 °C and 300 °C for 1 h. It was observed that when the pH was 6, the degradation rate increased with the annealing temperature and irradiation time reaching 51% at the annealing temperature of 300 °C and exposure time of 240 min. In other hands, when the pH was 10, and the sample was annealed at 200 °C, it showed a good degradation rate of 100% at the irradiation time of 90 min. By contrast, the sample annealed at 300 °C required 180 min to degrade the MB dye completely. The photoelectrochemical cell measurement based on photocurrent density revealed a slight response to light. Cycle voltammetry (CV) measurement was conducted, and the CV curves of the Ag/ZnO core/shell electrodes indicated nonfaradaic and pseudocapacitance behavior. The electrodes showed nearly rectangular CV curves, which indicated the dominance of the nonfaradaic capacitance behavior. The specific capacitance of the electrodes remained at approximately 99%. Mott–Schottky analysis revealed that the semiconductor was an n-type with dependence on flat band potential V_{FB} deviation in the negative direction.

Keywords: ZnO, core/shell, photocatalyst, photoelectrochemical cell

(Some figures may appear in colour only in the online journal)

1. Introduction

Zinc oxide (ZnO) nanostructure is considered as a promising photocatalytic material due to its high catalytic activity, low cost, environmental friendliness, chemical stability, and easy synthesis in nanostructured forms. The main limitation of the ZnO nanostructure in achieving a high photocatalytic efficiency is the rabid recombination of charge carriers. Hence, the design and modification of ZnO photocatalysts with high sensitivity and reactivity has attracted increasing attention.

* Author to whom any correspondence should be addressed.

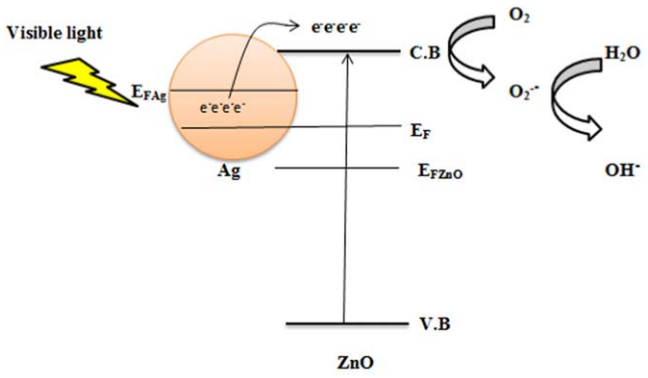

Figure 1. Proposed schematic illustrations of the band structure related photocatalytic mechanism for the Ag/ZnO heterojunction.

Existing studies have found that photocatalytic performance can be greatly improved by developing different composites and structures based on ZnO [1, 2].

ZnO has a wide band gap of 3.37 eV and high exciton binding energy of 60 meV. ZnO nanostructures such as ZnO nanorods have excellent properties, such as high sensitivity to surface oxygen adsorption, excellent electron transport, large surface area-to-volume ratio and specific crystalline orientation [2–5]. However, the wide band gap of semiconductors such as ZnO and TiO_2 that are used as photocatalytic materials make them undesirable to use under UV light [6–8]. Therefore, replacing UV light with visible light to catalyze organic pollutants has become an urgent requirement [6, 9].

The catalytic activity of ZnO under visible light can be improved by modifying ZnO with noble metals [6], such as Cd [10], Cu [11], Au [9, 10] Ag [11, 12], and Pt [13, 14]. Silver (Ag) can be used to modify ZnO to enhance its photocatalytic activity. Ag/ZnO being an important structure for the reduction of Ag^+ due to the high consequent quantum yield of Ag nanoparticles (NPs) [6, 7]. Metal/semiconductor core/shell structure such as Ag/ZnO shows surface plasmon resonance (SPR) phenomena and the coherent oscillation of free electrons in resonance with the incident light; these property enhances photocatalytic efficiency due to increasing light absorption and scattering in addition to inducing charge separation in semiconductors [15]. SPR of Ag NPs is located at visible wavelength that lead to matches the excitation light [16]. However, a Schottky junction can be formed between metallic NPs and semiconductors. The equilibrium alignment of the Fermi levels of metal and semiconductor materials creates a built-in electric field in the space-charge region near the interface, and this property can promote the separation of photogenerated electrons and holes [17]. The enhancement of photocatalysts is due to the generation of numerous free holes in the valance band (VB) that lead to active oxygen species, such as OH^- radicals and O_2^-, being generated by electrons in the condition band (CB); these species are mainly responsible for dye degradation [6, 18, 19] as shown in figure 1.

Photoelectrochemical cells (PECs) have attracted important attention because of their potential to be adopted as sustainable and renewable technology for harvesting and converting solar energy and for their wide applications in water splitting [15]. The photocatalyst absorbs photon energy larger than their band gap energy, and it generates pairs of light-excited charging carriers. The separated charges travel to different locations from the photocatalyst surface without recombination. At these locations, water and oxidation are reduced by the photoexcited charge carriers to produce H_2 and O_2. The first two steps depend heavily on the structural and electronic properties of the photocatalyst while the third step is strengthened by the presence of a solid catalyst [17]. In the present work, Ag/ZnO core/shell nanostructures are prepared by chemical reduction, and their photocatalytic activity against methylene blue (MB) dye is investigated under visible light with different pH values, annealing temperatures, and PEC properties.

2. Experimental

2.1. Ag/ZnO core/shell synthesis

ZnO nanorods were prepared by chemical bath deposition (CBD) following two steps [20]. First, the ZnO seed layer solution was prepared using 5 mM of zinc acetate dihydrate [$Zn(CH_3CO_2)_2 \cdot 2H_2O$] dissolved in 50 ml of ethanol with stirring for 3 h at room temperature. The seed solution was casted on clean glass substrates and FTO/glass and then dried at 50 °C. The seeded substrates were annealed at 350 °C for 1 h to grow ZnO NPs and were left to cool naturally to room temperature.

Second, ZnO nanorods were grown onto seed layers by CBD. The seeded substrates were immersed vertically inside a beaker containing 0.1 M each of zinc nitrate hexahydrate [$Zn(NO_3)_2.6H_2O$] and hexamine ($C_6H_{12}N_4$) that were dissolved individually in 25 ml of distilled water at 70 °C. The produced nanorods grown at 90 °C for 2 h were dried and thermally annealed for 1 h at 350 °C.

To prepare Ag/ZnO core/shell thin films, ZnO nanorod thin films were soaked for 5 h in a solution contains Ag nanoparticles during preparation by electrochemical method through two pure silver electrodes for cell electric. The ZnO samples left in the solution for 19 h after power off. Then, Ag/ZnO core/shell thin films were dried at room temperature, and some samples were annealed at 200 °C and 300 °C for 1 h. Schematic of preparation steps are shown in figure 2.

2.2. Photocatalytic activity measurements

The photocatalytic activity of the prepared Ag/ZnO core/shell thin films was investigated using an aqueous solution of MB dye prepared with a concentration of 9 ppm. The prepared Ag/ZnO thin films were placed in a beaker containing 40 ml of MB dye solution and exposed to white light with an intensity of 0.33 mW cm^{-2}.

The degradation ratio of MB dye solution was determined using various pH values, temperatures and exposure times. The degradation rate of MB dye was determined using the following formula [21]:

$$\text{Degradation rate}(\%) = \frac{A_o - A}{A_o} \times 100\%, \qquad (1)$$

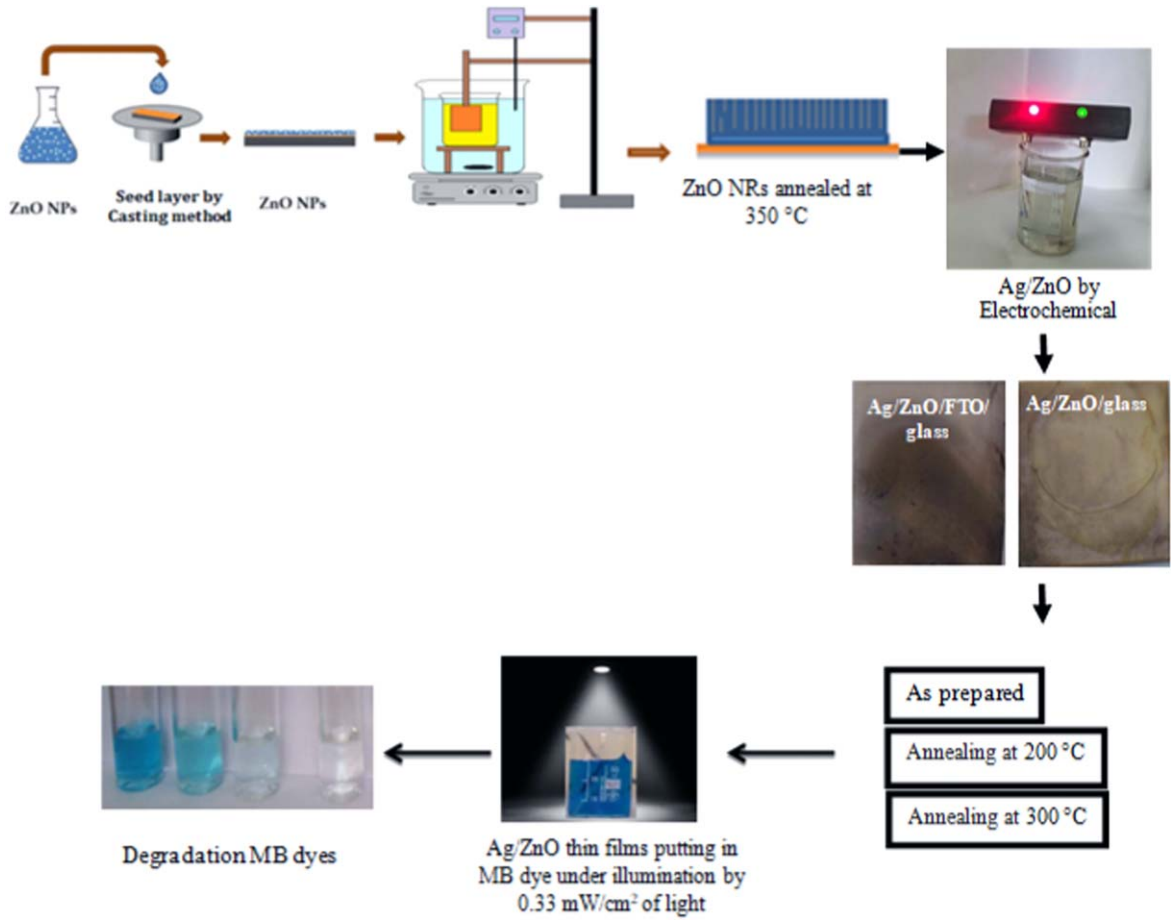

Figure 2. Schematic of photocatalysis process experiment.

where A_o, A are the absorbance values before and after exposure to white light for several minutes, respectively.

The pH value of the MB dye solution was set using NaOH and a few drops of HNO_3 acid. The pH value determines the surface charge of the photocatalytic material, that is, the surface charge is positive in an acidic medium and negative in a basal medium [1]. In this experiment, the pH was set to 6 for the acidic medium and 10 for the alkaline medium. The degradation kinetics (k) of the MB dye can be described using pseudo first-order kinetic model given by [9]

$$\ln\left(\frac{C}{C_o}\right) = -kt, \tag{2}$$

where $\boldsymbol{t}$ is the reaction time, $\boldsymbol{C_o}$ is the initial concentration of the MB dye, $\boldsymbol{C}$ is the concentration after of exposure, and $\boldsymbol{k}$ is the first-order constant of the degradation reaction. The concentration is calculated according to Beer–Lambert's law given by [22]:

$$A = \varepsilon\, C\, l, \tag{3}$$

where $\boldsymbol{A}$ is the absorbance, $\boldsymbol{\varepsilon}$ is the molar absorptivity, and $\boldsymbol{l}$ is the UV light path length (1 cm).

2.3. PEC measurement

Ag/ZnO/FTO was characterized using PEC consisting of three electrodes: working electrode measuring (1.5 × 2.5) cm, counter electrode made of Pt plate measuring (1 × 1) cm, and a reference electrode made of Ag/AgCl (KCl saturated). Exactly 1.0 M of KOH solution with pH of 13.6 was used as the electrolyte, and the working electrode was illuminated by white light with an intensity of 0.33 mW cm^{-2} from the front in all measurements.

The three electrodes of the cell were connected to an electrical circuit for PCStrace5 version 5.6, lamSens compact electrochemical interfaces.

2.3.1. Electrochemical performance measurement. Several measurements, including linear sweep voltammetry (LSV) and cycle voltammetry (CV), were performed to evaluate the cell performance.

The positive and negative potential windows were +0.5 V to −0.5 V versus Ag/AgCl. LSV measurement (J−V curves) was performed under light and dark conditions with a scan rate of 0.05 V s^{-1} to measure the J–V characteristics in the electrolytes of 1 M of KOH.

Photoconversion efficiency was estimated as [23]

$$\eta = \frac{J_{\mathrm{ph}} \times (1.23 - V_{\mathrm{b}})}{P_{\mathrm{total}}}, \tag{4}$$

where J_{ph}, P_{total}, and V_b are the photocurrent density, power density of light irradiation, and applied voltage versus hydrogen reference electrode, respectively. The CV test under dark conditions was conducted six times using scan rates of 0.05, 0.1, 0.2, 0.3, 0.4, and 0.5 V s^{-1} for two cycles.

2.3.2. Mott–Schottky measurement. The Mott–Schottky plot was measured under dark conditions to determine the charge carrier density (N_D) for the photoanode and the flat band potential (V_{FB}) of a thin film photoelectrode. Mott–Schottky theory is used to analyze the interfacial capacitance of the semiconductor-liquid junction through the following equation [24]:

$$\frac{1}{C^2} = \frac{2}{e\varepsilon\varepsilon_0 N_D}\left(V_A - V_{FB} - \frac{KT}{e}\right), \tag{5}$$

where C, ε_0, ε, e, V_A, k, and T represent the space charge capacitance (F cm^{-2}), vacuum permittivity (8.854×10^{-14} F cm^{-1}), dielectric constant of semiconductor (10 for ZnO) [24], electron charge (1.6×10^{-19} C), applied potential, Boltzmann constant (1.38×10^{-23} J K^{-1}), and temperature ($kT/e = 0.026$ V at room temperature), respectively. The Mott–Schottky measurements were performed using applied bias voltage with different frequencies of 100, 1000, and 10 000 Hz.

Donor density N_d can be calculated from the Mott–Schottky plot on the basis of the slope using the following equation [22, 23]:

$$N_D = \frac{2}{e\varepsilon\varepsilon_0}[d(1/C^2)/dV]^{-1}, \tag{6}$$

$$V_{FB} = V_A - 0.026. \tag{7}$$

Depending on the value of N_D, the space charge layer width (W), also called the depletion layer at the semiconductor/electrolyte interface, was calculated by [21, 24]

$$W = \left(\frac{2\varepsilon\varepsilon_o(V - V_{FB})}{eN_D}\right)^{1/2}. \tag{8}$$

The Fermi level (E_F) was calculated with the following equation [25]:

$$E_F = -eV_{FB} \tag{9}$$

On the basis of the values of E_{FB} and band gap E_g, the conduction band minima (E_{CB}) and valence band maxima (E_{VB}) can be calculated using the following equations:

$$E_{CB} = E_F - kT\ln\left(\frac{N_D}{N_C}\right), \tag{10}$$

$$E_g = E_{CB} - E_{VB}, \tag{11}$$

where N_C represents the effective density of the states at the bottom of the conduction band; it is given by

$$N_C = 2\left(\frac{2\pi m_n^* kT}{h^2}\right)^{3/2}, \tag{12}$$

where m_n^* is the electron effective mass ($m_n^* = 0.24m_o$ for ZnO) [26]. Through N_D, the Debye length (L_D) of the charge carriers, also known as the diffusion lengths of charge carriers, for the photoanode is [27]

$$L_D = \left(\frac{\varepsilon\varepsilon_o kT}{e^2 N_D}\right)^{1/2}. \tag{13}$$

2.3.3. Electrochemical impedance spectroscopy (EIS). EIS was performed to determine the electrical properties of the prepared Ag/ZnO core/shell thin films by using the same electrochemical workstation. EIS was measured under irradiation by white light for all electrodes. The AC voltage capacity was 0.01 V, and the DC voltage was 0.0 V. The frequency range was between (10^6) Hz and (0.1) Hz in dark and light conditions.

3. Results and discussion

3.1. Morphology and optical properties

Figure 3 shows the FESEM image of the Ag/ZnO core/shell thin film that grown onto glass and FTO/glass substrates. The FESEM images in figure 3 confirmed that ZnO nanorods are grown vertically onto surfaces of substrates. Further, the deposition of Ag NPs on ZnO nanorods revealed the core/shell structure were Ag NPs are covered ZnO NRs surface.

Figures 4(A) and (B) show the particle size distribution of the Ag NPs prepared by the electrochemical method and deposited on ZnO/glass NRs and ZnO/FTO thin films, respectively. The particle size of Ag that prepared onto ZnO/glass ranged from 3.5 to 41.7 nm with average particles size is 20 nm while it was ranged from 3.2 to 99 nm for Ag NPs that synthesized onto ZnO/FTO NRs with average size of 41 nm. Furthermore, Ag nanoparticles can be prepared using chemical reduction or green-synthesis to obtain average size around 50 nm for using as a catalyst to grow silicon nanowires [16]. However, electrochemical method could be led to prepare Ag nanoparticles with average particles size less than other methods.

Figure 5(A) shows the absorbance spectra for the as-prepared via CBD of Ag/ZnO/glass thin films and that annealed at 200 °C and 300 °C. All prepared samples are appeared high absorption to wavelengths in the UV region (<400 nm). As shown in figure 5(B), the band gap value for as-prepared Ag/ZnO and with annealing at 200 °C and 300 °C was 3.19, 3.22, and 3.25 eV, respectively. Pourshaban *et al* prepared ZnO nanorods onto soda lime glass substrates via CBD method and they found the energy band gap was 3.2 eV that closed with our obtained value [28]. However, increasing the band gap with increasing annealing temperature is could be due to increasing the oxygen ratio in the ZnO nanorods [29].

Figures 6(A) and (B) show the absorbance spectra and $(\alpha h\upsilon)^2$ versus $h\upsilon$ of the Ag/ZnO/FTO core /shell and that annealed at 200 °C and 300 °C. The absorbance of the as-prepared Ag/ZnO core/shell appeared higher compared by

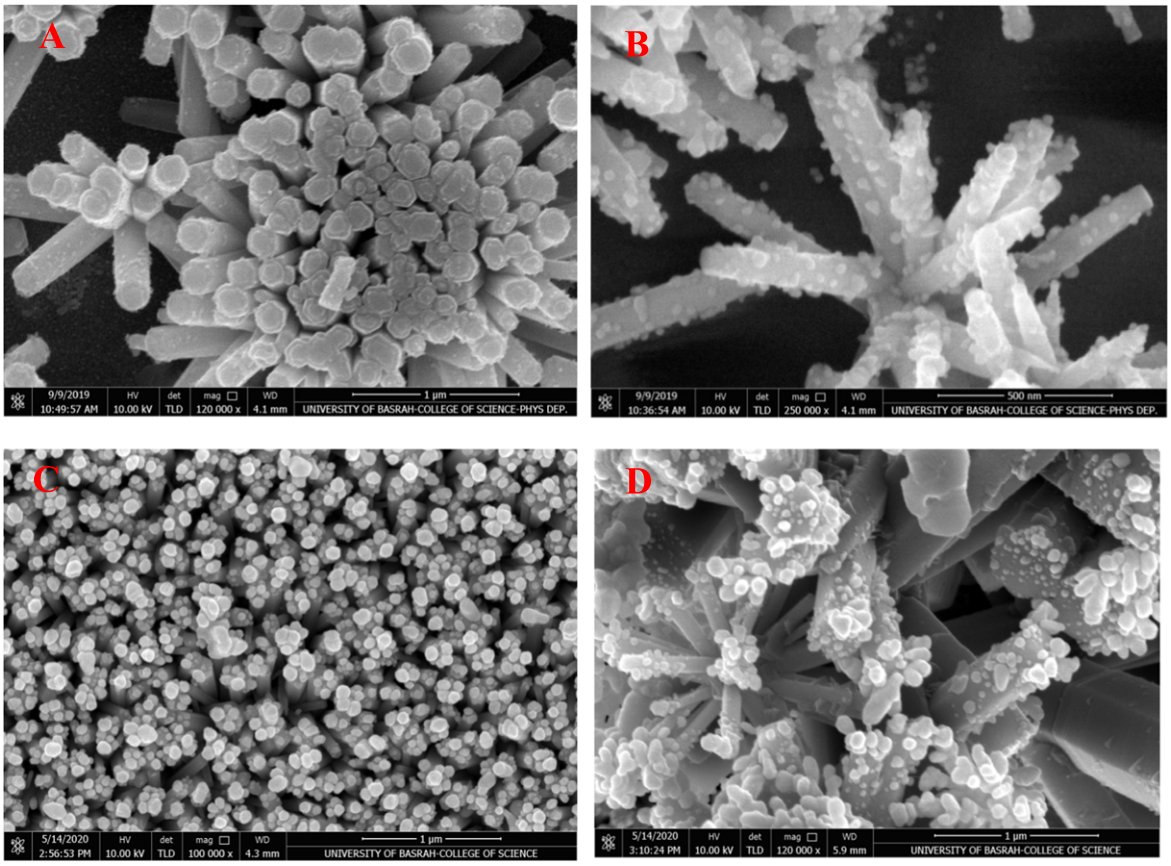

Figure 3. FESEM images of grown Ag/ZnO core–shell thin film (A) and (B) onto glass substrates, (C) and (D) onto FTO/glass substrate.

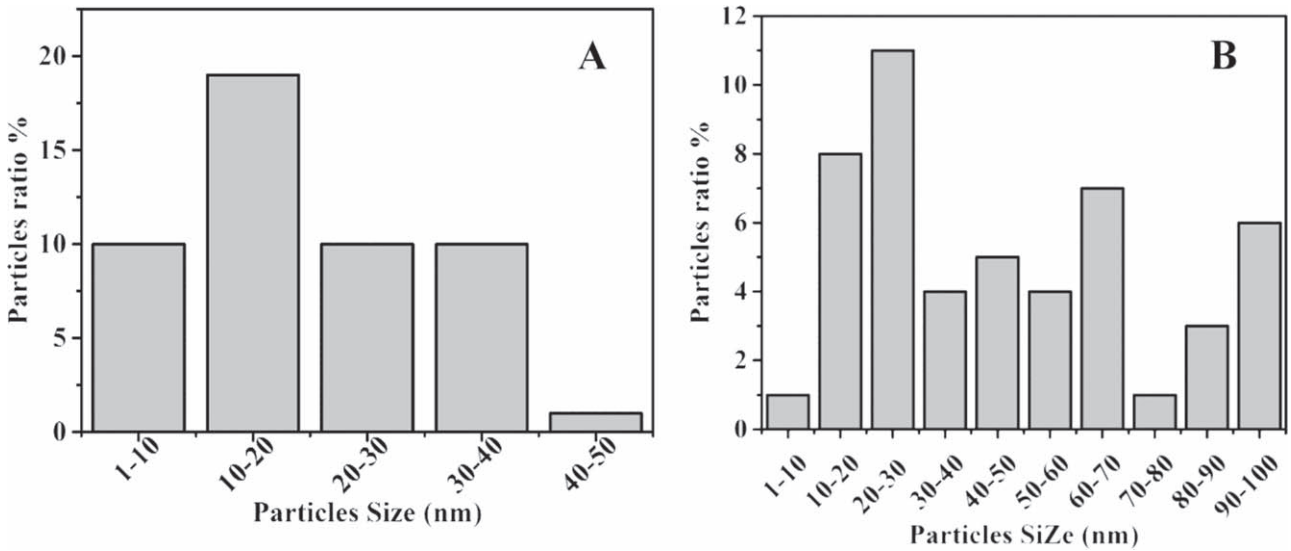

Figure 4. Statistical distribution of particles size of Ag NPs on (A) glass and (B) FTO/glass substrates.

those annealed at 200 °C and 300 °C. Note that the absorbance spectrum of the as-prepared Ag/ZnO return reason increase edge in state Ag/ZnO with annealing at 200 °C and 300 °C, which is comparable to the energy band gap reported by Tarwal and Patil [30]. Figure 6(B) shows that the energy band gaps of the as-prepared Ag/ZnO core/shell and that annealed at 200 °C and 300 °C was 3.05, 3.1, and 3.13 eV, respectively. However, obtained values of energy gap of Ag/ZnO core/shell nanostructure is close to Ag/TiO_2 nanostructure that effectively used as a photocatalyst material [7].

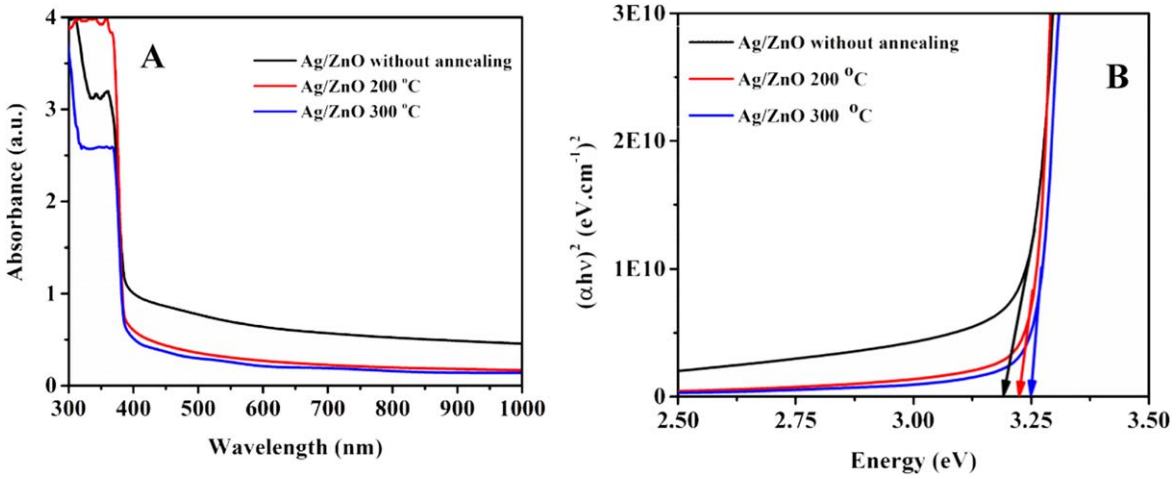

Figure 5. (A) UV–vis spectra for Ag/ZnO thin film onto glass substrate (B) the plot of $(\alpha h\upsilon)^2$ versus photon energy.

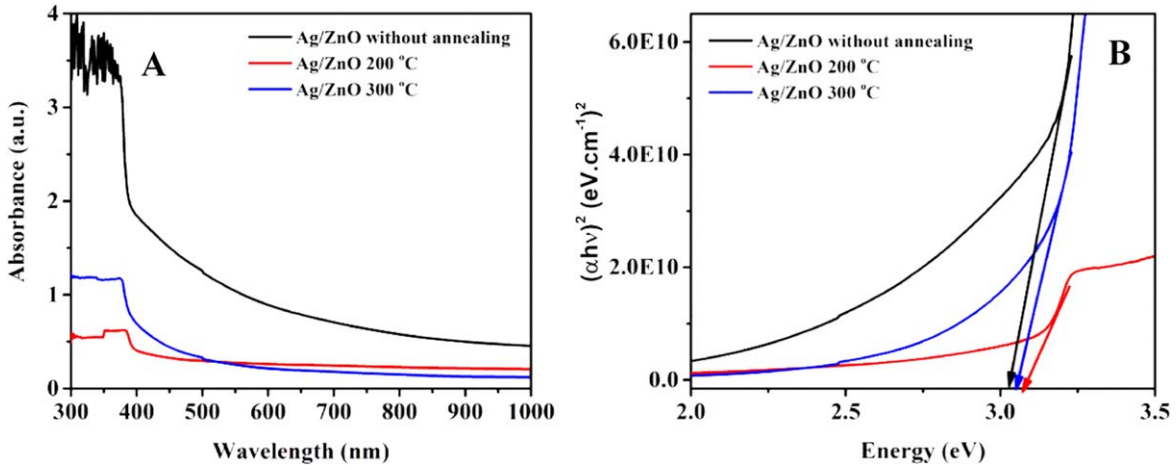

Figure 6. (A) Effect of annealing temperature on the UV–vis spectra of Ag/ZnO thin films onto FTO/glass substrate (B) the plot of $(\alpha h\upsilon)^2$ versus photon energy.

3.2. Photodegradation of MB dye

Figures 7(A)–(C) shows the absorbance of MB dye for the three samples of as-prepared Ag/ZnO and those annealed under 200 °C and 300 °C given a pH value. Figures 8(A)–(C) show the absorbance of MB dye for the three samples of as-prepared Ag/ZnO and those annealed at 200 °C and 300 °C under a pH value of 10 and under various exposure times (30–240 min). The effect of pH on the rate of degradation was studied for the MB dye, with the pH value playing an important role in the efficiency of photocatalytic degradation. The absorbance of MB dye decreases with increasing irradiation time, thereby increasing the degradation efficiency of photocatalysts [31].

The degradation rates (%) of MB dye under the effect of Ag/ZnO thin films at pH 6 and 10 are shown in figures 9(A) and (B), respectively. The degradation rate increased under an alkaline medium because of the increase in hydroxyl ions that stimulate the formation of hydroxyl radicals OH^- in alkaline conditions [32]; this change leads to the degradation of MB dye on the surface of reduced catalytic materials [33]. The degradation rates of MB dye under exposure time of 240 min and pH of 6 for the as-prepared Ag/ZnO and those annealed at 200 °C and 300 °C were 71%, 41%, and 51%, respectively. At pH 10, the degradation rates were 98% for the as-prepared Ag/ZnO thin film, 100% for Ag/ZnO annealed at 200 °C for 90 min, and 100% for Ag/ZnO annealed at 300 °C for 180 min. The results are aligned with those of T J Whang *et al* who reported degradation rates of 35%, 41%, and 92% for pH values of 4, 7, and 11 and exposure time of 8 h [34]. For a pH of 7, the degradation rate at 1 h was 97% [35]; by contrast, Fageria *et al* obtained a degradation rate of 40% at 2 h under the same pH [35]. However, other compounds such as N-doping Ta_2O_5 NFs can be used for degradation MB dye under white light [19].

In the heat treatment of Ag/ZnO annealed at 200 °C and 300 °C under a pH of 10, good degradation catalytic of AgO formation it can produce holes in light leading to hydroxyl radicals that break down the dye. This result might be due to

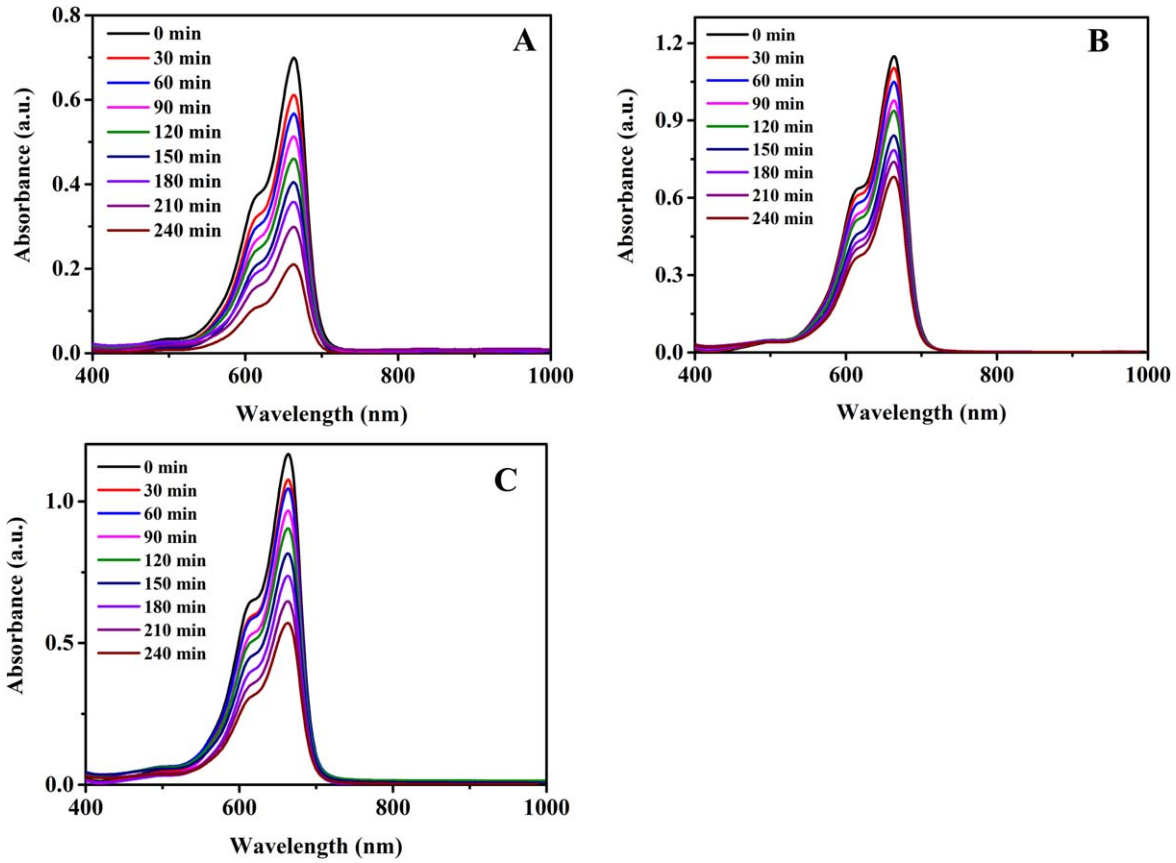

Figure 7. UV–vis spectra of MB dye of pH 6 effect photocatalytic degradation of (A) as prepared (B) with annealing 200 °C (C) with 300 °C Ag/ZnO/glass thin films.

the presence of AgO, a metal oxide, in the system [6, 31]. But Ag/ZnO with annealed 200 °C degradation rate rabid thin film with 300 °C, where it is expected that the bonds Ag–O will weaker than the bond Ag–Ag as the temperature increase. Furthermore, to evaluate stability of as prepared ZnO/Ag core–shell thin films in alkaline and acidic solution the degradation of MB dye measurement was repeated for three times using same sample after remove the dye from the surface of thin films by ethanol. The obtained results are excellent were we found that degradation rate is just degreased from 71% to 68% (4.2%) when pH is 6 and it was degreased from 98% to ~94% (3.7%) when the pH is 10. This point is very important because the sample can be used more than times without needing to filter solution as when nanopowder is used. Other important view point, wide area of ZnO/Ag thin films onto glass substrates can be used for degradation oil stain that could pollute ocean or seas.

In figures 10(A) and (B), which shows the—ln (C/C_o) plot versus irradiation time, the linear lines show that the photodegradation of MB dye by Ag/ZnO nanorods followed the k first-order kinetic reaction regardless of the annealing temperature and pH value used. The highest values of kinetic reaction (k) were noted in the samples of Ag/ZnO thin films in alkaline media annealed 200 °C and 300 °C and in the as-prepared Ag/ZnO under irradiation times of 90, 180, and 240 min are 0.0668 min^{-1}, 0.0286 min^{-1} and 0.0165 min^{-1}, respectively. While in state the acidic medium, the kinetic reaction k values were for the as-prepared Ag/ZnO, Ag/ZnO annealed at 200 °C, and Ag/ZnO annealed at 300 °C for 240 min are 0.0046, 0.0022 and 0.0029 min^{-1} respectively. The reason of low k values in acidic medium is at a high pH, dye adsorption increases as the amount of adsorption becomes proportional to the concentration of the substrate. In this case, the total rate is the same as the rate of adsorption of the substrate molecules, thereby resulting in surface reactions [36] and quick separation processes. This condition leads to increased reaction kinetics in alkaline media.

3.3. Photoelectrochemical properties

The J–V study was carried out on the Ag/ZnO core/shell nanorod photoelectrodes in dark and light states versus Ag/AgCl applied voltage. Figures 11(A) and (B) shows the LSV (J–V) result of the Ag/ZnO core/shell thin films under dark and white light illumination. The Ag/ZnO thin films showed the slight effect of light.

Under dark, the current density under 0.1 V bias voltage of the as-prepared Ag/ZnO core/shell and those annealed at 200 °C and 300 °C was 0.021, 0.015, and 0.066 $mAcm^{-2}$, respectively. Under white light irradiation, the photocurrent densities of the as-prepared Ag/ZnO core/shell and those annealed at 200 °C and 300 °C were 0.029, 0.018, and 0.026 mA cm^{-2}, respectively.

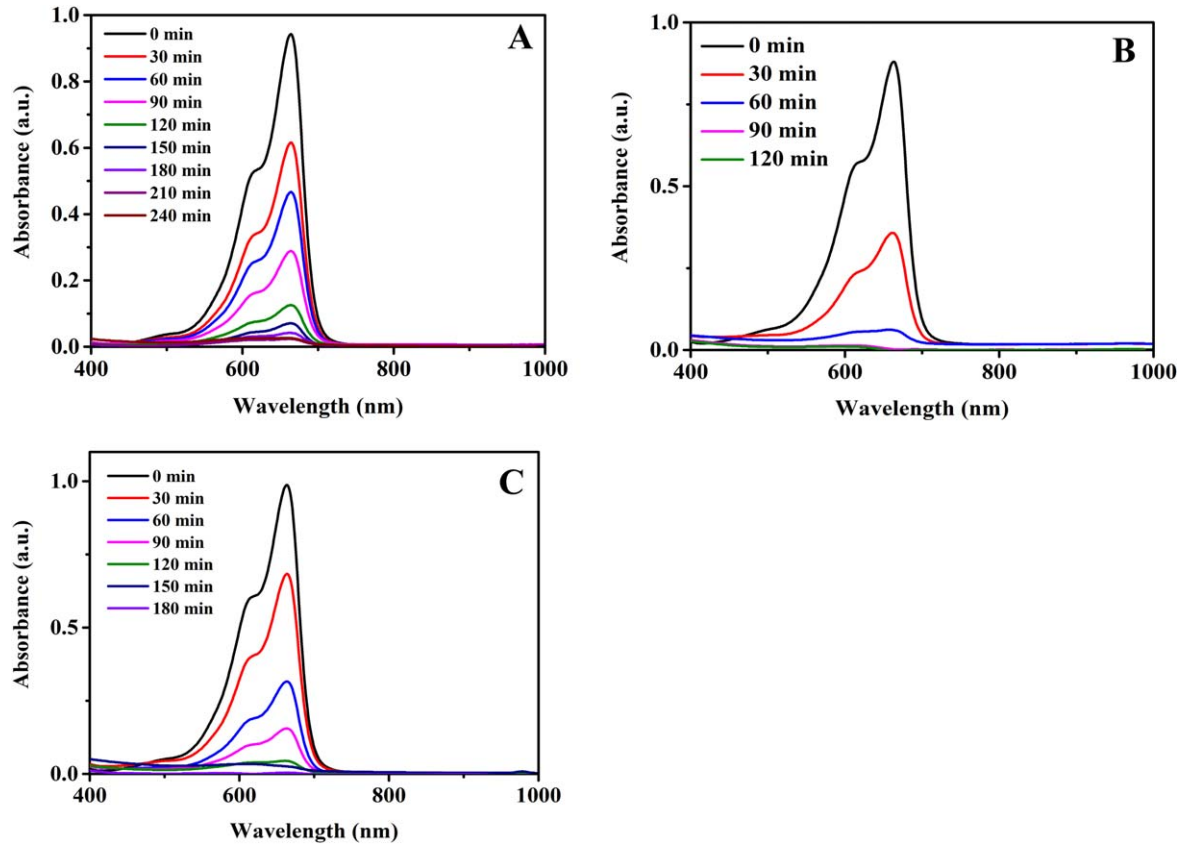

Figure 8. UV–vis spectra of MB dye of pH 10 effect photocatalytic degradation of (A) as prepared (B) with annealing 200 °C (C) with 300 °C Ag/ZnO/glass thin film.

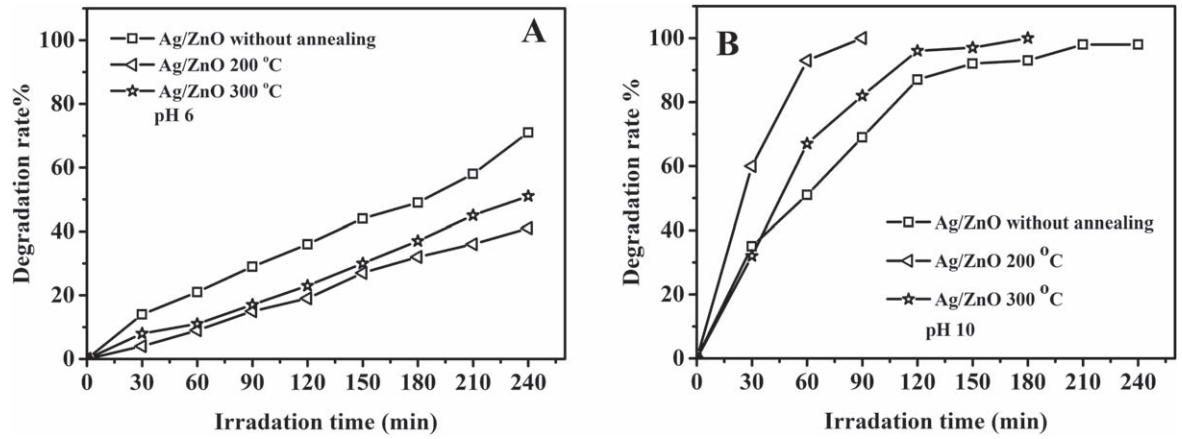

Figure 9. Degradation rate% of MB under effect Ag/ZnO/glass thin films at (A) pH 6 (B) pH 10 influence.

The photoconversion efficiency (η) of the prepared ZnO nanorods and Ag/ZnO core/shell under illumination by white light is shown in figure 12 and is derived according to equation (4) at 0.1 V applied bias versus Ag/AgCl.

The as-prepared Ag/ZnO showed a η value of 0.1 while those annealed at 200 °C and 300 °C showed the same η value of 0.06. These results are in accordance with those of previous research under white light (table 1).

The CV experiment under dark conditions was repeated six times using different scan rates of 0.05, 0.1, 0.2, 0.3, 0.4, and 0.5 V s^{-1}. Figures 13(A) and (B) show the CV curves of the Ag/ZnO core/shell nanorod electrodes, which exhibited nonfaradaic and pseudocapacitance behavior. The CV curves showed reversible peaks and a nearly rectangular shape, which indicated the dominance of the nonfaradaic capacitance behavior because the charge is stored in the electrolyte dissolved interface. However, under 0.3 V s^{-1} (figure 13(C)), the cathodic peak occurred near 0.0 V versus Ag/AgCl in the positive potential due to the faradaic reaction. The as-prepared Ag/ZnO core/shell nanorods demonstrated good

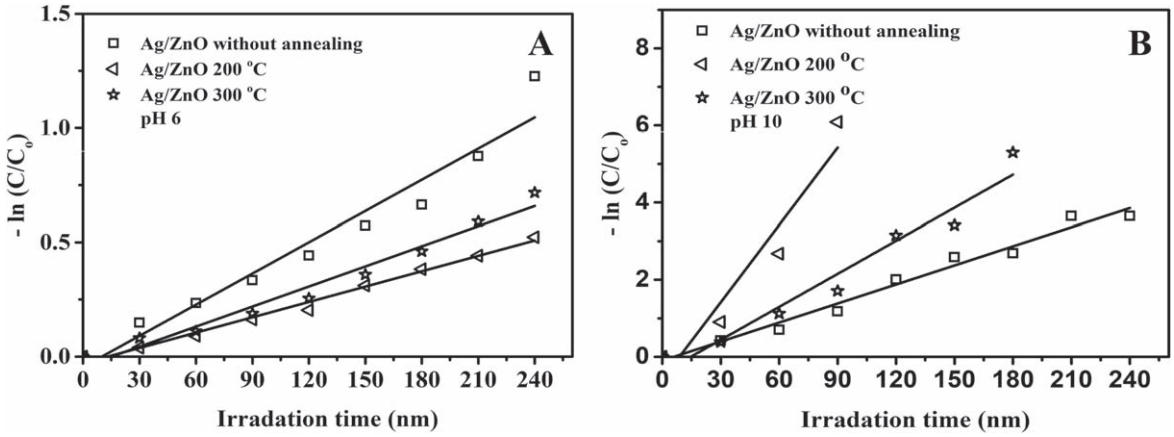

Figure 10. Variation of $-\ln(C/C_o)$ with irradiation time at (A) pH 6 (B) pH 10 of Ag/ZnO/glass thin films.

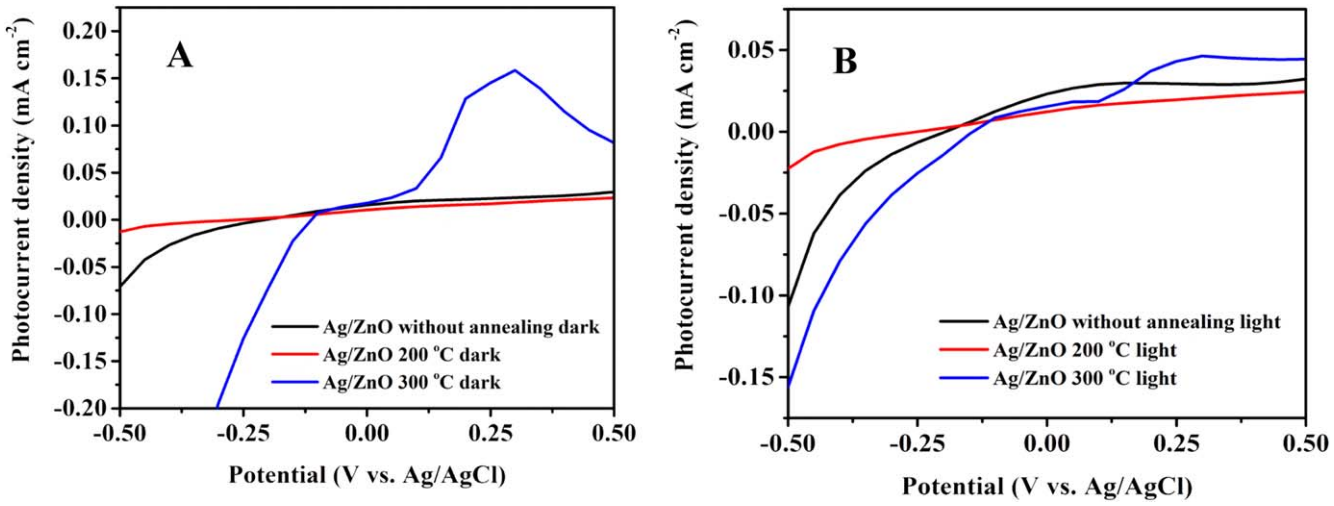

Figure 11. Linear sweep voltammetry (I–V) of Ag/ZnO/FTO thin film at (A) dark (B) light conditions.

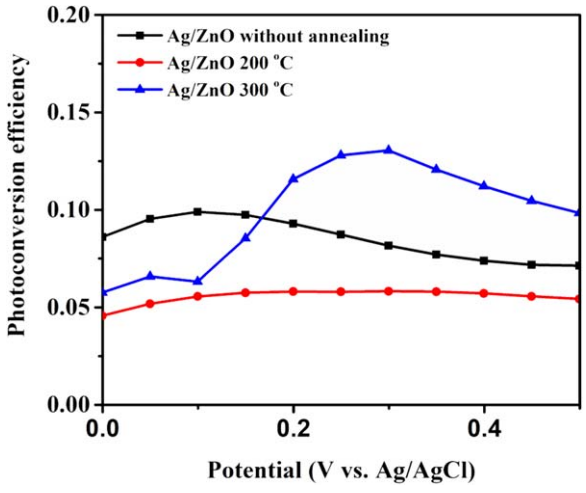

Figure 12. Photoconversion efficiency as a function to potential of Ag/ZnO/FTO thin film.

capability, good cycling performance, and fast charging process. According to Al-Asadi *et al* the absence of oxidation and reduction peaks is due to several reasons, including short lifetime separations, rapid reaction for redox process, and reversibility. In the case of good electrical conductivity, the redox sites are electrically coupled and provide most of the sites on the surface to circumvent solid ion diffusion. The electrodes are charged and discharged quickly at pseudo-constant rates through the perfect voltammetric cycle [39].

From real capacitance C_s measured stability of the electrodes according to [40]

$$C_s = \frac{\text{area under cycle}}{2SV\Delta V}, \tag{14}$$

where S is the area of the photoelectrode, V is the scan rate, and ΔV is the potential window for the electrolyte. All synthesis electrodes were measured for 250 cycles within the mounted potential windows. The scan rate was 0.5 V s^{-1}, and the step size was 0.05 V for the areal capacitance (figure 14). The areal capacitance of the electrode remained at approximately 99% for the as-prepared Ag/ZnO and those annealed at 200 °C and 300 °C. Hence, the initial value after 250 charge and discharge cycles explained the excellent long-term cycling stability of the electrodes.

The areal capacitance decreased as the scan rate increased from 0.05 to 0.5 V s^{-1} for the Ag/ZnO thin films. The highest C_s was achieved at a scan rate of 0.05 V s^{-1}. For

Table 1. Approach for previous publications.

Photoanode	Electrolyte	Con. (M)	P (mW cm^{-2})	η	V_{Bais}(V)	Substrate	References
Ag/ZnO	KOH	0.1	1	0.26	0.4	ITO	[37]
Ag/Co-ZnO	KOH	0.1	1	0.73	0.6	ITO	[37]
Ag/ZnO	Na_2SO_4	0.5	100	0.81	0.29	PET	[38]
As prepared Ag/ZnO core/shell	KOH	1	0.33	0.1	0.1	FTO	This study
Ag/ZnO with annealed 200 °C	KOH	1	0.33	0.06	0.1	FTO	This study
Ag/ZnO with annealed 300 °C	KOH	1	0.33	0.06	0.1	FTO	This study

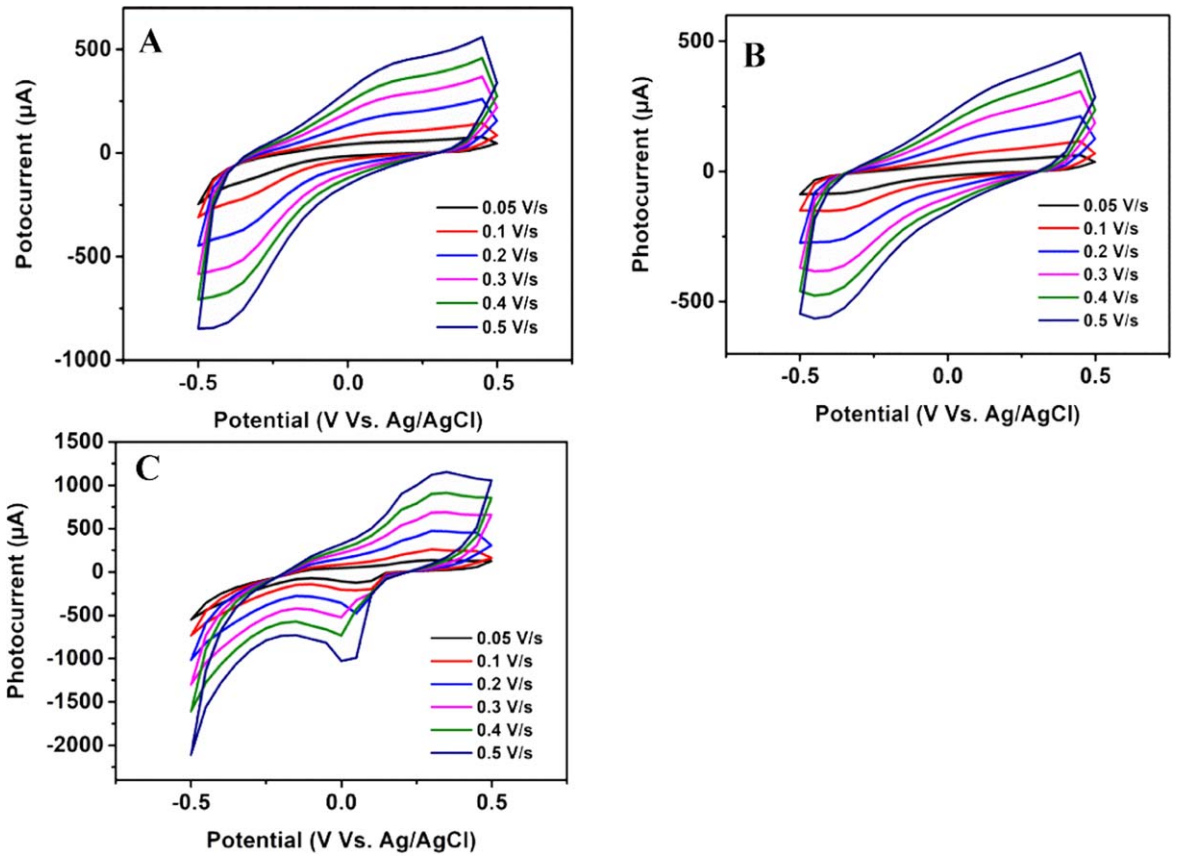

Figure 13. CV of (A) as prepared (B) annealed at 200 °C (C) 300 °C Ag/ZnO/FTO thin film electrode using different scan rate.

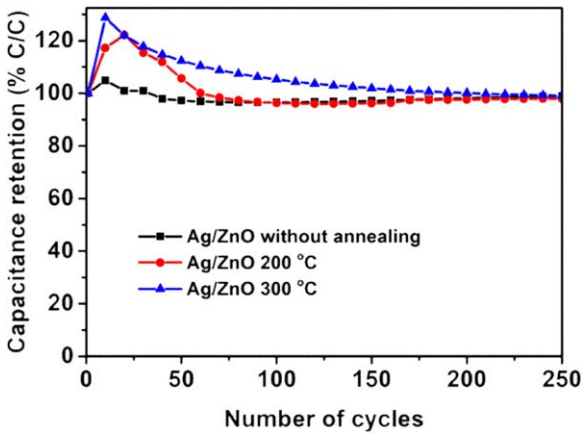

Figure 14. Percent capacitance retained by Ag/ZnO/FTO thin film electrode 250 cycles.

ZnO, C_s was 224 F cm^{-2}; for the as-prepared Ag/ZnO, Ag/ZnO annealed at 200 °C, and Ag/ZnO annealed at 300 °C, the C_s values were 164, 135, and 278 F cm^{-2}, respectively.

The areal capacitance decreased with increasing scan rate due to the slow ion diffusion and increased scan rate that caused a rapid decrease in the concentration of electrical ions on the electrode surface. The area of the inner surface of the electrode has an important role in this process as the area of the lower surface is involved in electrochemical processes at high scan rates [41].

The result of the Mott–Schottky measurement is shown in figures 15(A)–(C), where the Mott–Schottky in equation (5) is plotted as a function of the applied bias voltage.

Figure 15(A) presents the Mott–Schottky plots of the Ag/ZnO core/shell thin films under a frequency of 100 Hz. The figure shows that not all plots are linear but that linearity

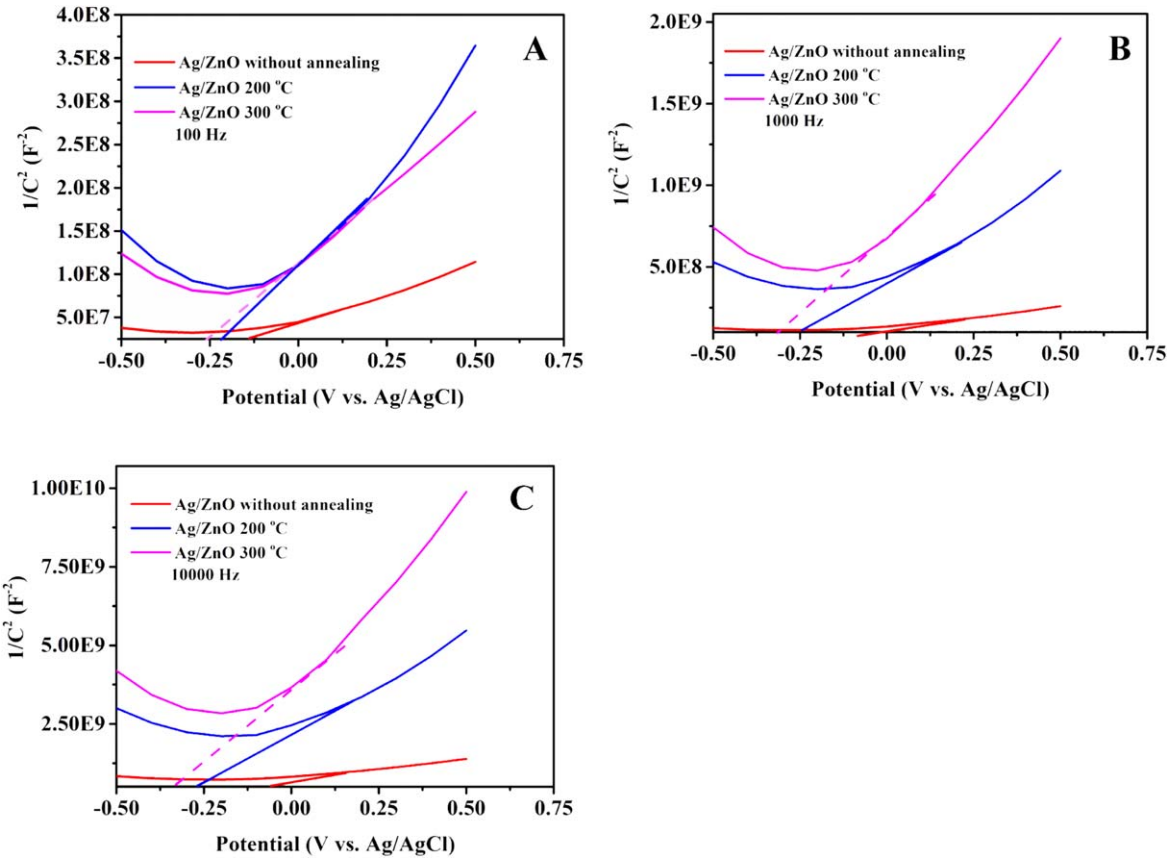

Figure 15. Mott–Schottky plots of the pristine Ag/ZnO/FTO at a frequency of (A) 100 Hz (B) 1000 Hz (C) 1000 Hz in the dark.

appears after an interval of approximately −0.3 to 0.5 V versus Ag/AgCl. Through the data in the linear part of all samples, the flat band potentials (V_{FB}) of the photoanode electrodes could be estimated. The flat band potentials were −0.13, −0.22, and −0.26 for the as-prepared Ag/ZnO core/shell thin films and those annealed at 200 °C and 300 °C, respectively.

From the linear part, the slope representing the donor density (N_D) for each sample. The N_D values were 1.8×10^{23}, 6.2×10^{22}, and 6.6×10^{22} cm^{-3} for as-prepared Ag/ZnO core/shell thin films and those annealed at 200 °C and 300 °C, respectively. These results are consistent with those of Ortega *et al* [42], who reported an N_D equal to 13.07×10^{22} cm^{-3}. Further, the positive Mott–Schottky slope indicated that the semiconductor was n-type [42]. Figure 15(B) shows the Mott–Schottky plots of the Ag/ZnO core/shell thin films under a frequency of 1000 Hz and the linearity appeared after an interval of approximately −0.25 to 0.5 V versus Ag/AgCl. The flat band potentials were −0.097, −0.25, and −0.32 for the as-prepared Ag/ZnO core/shell thin films and those annealed at 200 °C and 300 °C, respectively. Moreover, the N_D values were high at 1.0×10^{23}, 2.4×10^{22}, and 9.6×10^{21} cm^{-3} for the as-prepared Ag/ZnO core/shell thin films and those annealed at 200 °C and 300 °C, respectively. Figure 15(C) shows the Mott–Schottky plots of the Ag/ZnO core/shell thin films under a frequency of 10 000 Hz. For this sample, the linearity appeared after an interval of approximately −0.25 to 0.5 V versus Ag/AgCl and the estimated V_{FB} values are −0.01, −0.27, and −0.33 for the as-prepared Ag/ZnO core/shell thin films and those annealed at 200 °C and 300 °C, respectively. In addition, the N_D values were high at 2.4×10^{22}, 5.3×10^{21}, and 1.9×10^{21} cm^{-3} for the as-prepared Ag/ZnO core/shell thin films and those annealed at 200 °C and 300 °C, respectively.

In general, the as-prepared and annealed Ag/ZnO core/shell thin films showed that flat band potentials V_{FB} do not depend on oxidation temperature and all obtained values were negative, as shown tables 2–4. This result fulfilled the Nernst equation and indicated the good performance of the photoanode electrode in the easy charge separation of photogenerated charge carriers and improvement of water splitting [43].

The as-prepared and annealed Ag/ZnO core/shell thin films showed low donor densities when frequencies increased to from 100 to 10 000 Hz (tables 2–4). The high donor density at low frequencies is aligned with the data on the capacitance from surface states at such frequencies reported by Akikusa and Khan, who also attributed the condition to the high number of oxygen vacancies within the crystallites formed at a high oxidation temperature [44]. Dielectric relaxation of semiconductors has been considered to be responsible for such a phenomenon and because they were considered of the origin dependent of frequency for the M–S plot has not well known [44]. The increase in donor density is considered as the degree of band bending at the nearness of the semiconductor surface, leading to the improvement of charge separation efficiency, which enhances photocurrent density under irradiation [45].

Table 2. Mott–Schottky parameters of Ag/ZnO core/shell nanorods at frequency of 100 Hz.

Sample	N_D (cm^{-3})	V_{FB} (V)	W (nm)	E_F (eV)	E_{CB}(eV)	E_{VB}(eV)	L_D(cm)
As prepared Ag/ZnO core/shell	1.8×10^{23}	−0.13	0.04	2.1×10^{-20}	−1.609	−4.629	9×10^{-10}
Ag/ZnO 200 °C	6.2×10^{22}	−0.22	0.08	3.5×10^{-20}	−1.581	−4.621	2×10^{-9}
Ag/ZnO 300 °C	6.6×10^{22}	−0.26	0.08	4.1×10^{-20}	−1.583	−4.653	2×10^{-9}

Table 3. Mott–Schottky parameters of Ag/ZnO core/shell nanorods at frequency of 1000 Hz.

Sample	N_D (cm^{-3})	V_{FB} (V)	W (nm)	E_F (eV)	E_{CB}(eV)	E_{VB}(eV)	L_D(cm)
As prepared Ag/ZnO core/shell	1.0×10^{23}	−0.097	0.05	1.6×10^{-20}	−1.594	−4.614	1.2×10^{-9}
Ag/ZnO 200 °C	2.4×10^{22}	−0.25	0.13	3.9×10^{-20}	−1.557	−4.597	2.4×10^{-9}
Ag/ZnO 300 °C	9.6×10^{21}	−0.33	0.22	5.2×10^{-20}	−1.533	−4.603	4×10^{-9}

Table 4. Mott–Schottky parameters of Ag/ZnO core/shell nanorods at frequency of 10 000 Hz.

Sample	N_D (cm^{-3})	V_{FB} (V)	W (nm)	E_F (eV)	E_{CB} (eV)	E_{VB} (eV)	L_D(cm)
As prepared Ag/ZnO core/shell	2.4×10^{22}	−0.05	0.08	8×10^{-21}	−1.557	−4.577	2.4×10^{-9}
Ag/ZnO 200 °C	5.3×10^{21}	−0.27	0.28	4.3×10^{-20}	−1.518	−4.558	5.2×10^{-9}
Ag/ZnO 300 °C	1.9×10^{21}	−0.33	0.50	5.3×10^{-20}	−1.491	−4.561	9×10^{-9}

An increase in donor density leads to the conversion of a semiconductor material into a conductor material in a process called metallization of semiconductors. This metallization process decreases the width of the space charge region where the field drop exists, consequently lowering the photocurrent density [44]. The calculated width of space charge region (W) from equation (8) depended on N_D at 100 Hz and was equal to 0.04, 0.08, and 0.08 nm for the as-prepared Ag/ZnO and those annealed at 200 °C and 300 °C, respectively. At 1000 Hz, the calculated space charge region was equal to 0.05, 0.13, and 0.08 nm for the as-prepared Ag/ZnO and those annealed at 200 °C and 300 °C, respectively. At 10 000 Hz, the calculated space charge region was equal to 0.08, 0.28, and 0.50 nm or the as-prepared Ag/ZnO and those annealed at 200 °C and 300 °C, respectively. All results are shown in tables 2–4.

Hence, the Fermi energy E_F calculated from equation (9) at 100 Hz was (2.1, 3.5, and 4.1) $\times 10^{-20}$ eV for the as-prepared Ag/ZnO and those annealed at 200 °C and 300 °C, respectively. At 1000 Hz, the Fermi energy E_F was (1.6, 3.9, and 5.2) $\times 10^{-20}$ eV for the as-prepared Ag/ZnO and those annealed at 200 °C and 300 °C, respectively. At 10 000 Hz, the Fermi energy E_F was (8, 4.3, and 5.3) $\times 10^{-20}$ eV for the as-prepared Ag/ZnO and those annealed at 200 °C and 300 °C, respectively. The conduction bands at 100 Hz calculated from equation (10) were −1.609, −1.581, and 1.583 eV for the as-prepared Ag/ZnO and those annealed at 200 °C and 300 °C, respectively. At 1000 Hz, the conductions bands were −1.594, −1.557, and −1.533 eV for the as-prepared Ag/ZnO and those annealed at 200 °C and 300 °C, respectively. At 10 000 Hz, the conduction bands were −1.557, −1.518, and −1.491 eV for the as-prepared Ag/ZnO and those annealed at 200 °C and 300 °C, respectively. The valence bands at 100 Hz calculated from equation (11) were −4.629, −4.621, and −4.653 eV for the as-prepared Ag/ZnO and those annealed at 200 °C and 300 °C, respectively. At 1000 Hz, the valence bands were −4.614, −4.597, and −4.603 eV for the as-prepared Ag/ZnO and those annealed at 200 °C and 300 °C, respectively. At 10 000 Hz, the valence bands were −4.577, −4.558, and −4.561 eV for the as-prepared Ag/ZnO and those annealed at 200 °C and 300 °C, respectively.

The calculated Debye length L_D at 100 Hz was (0.9, 2, and 2) $\times 10^{-9}$ cm for the as-prepared Ag/ZnO and those annealed at 200 °C and 300 °C, respectively. At 1000 Hz, the calculated Debye length L_D was (1.2, 2.4, and 4) $\times 10^{-9}$ cm for the as-prepared Ag/ZnO and those annealed at 200 °C and 300 °C, respectively. At 10 000 Hz, the calculated Debye length L_D was (2.4, 5.2, and 9) $\times 10^{-9}$ cm for the as-prepared Ag/ZnO and those annealed at 200 °C and 300 °C, respectively. The highest Debye length among all compound nanostructures was observed at high frequencies. According to Nazarov *et al* the Debye length for ZnO is assumed accepted that about 0.07 μm [46] while Asha *et al* the Debye for ZnO samples are (1.31–1.84) nm [47].

The electrochemical impedance spectra (Nyquist plot) of all the samples are shown in figures 16(A)–(C).

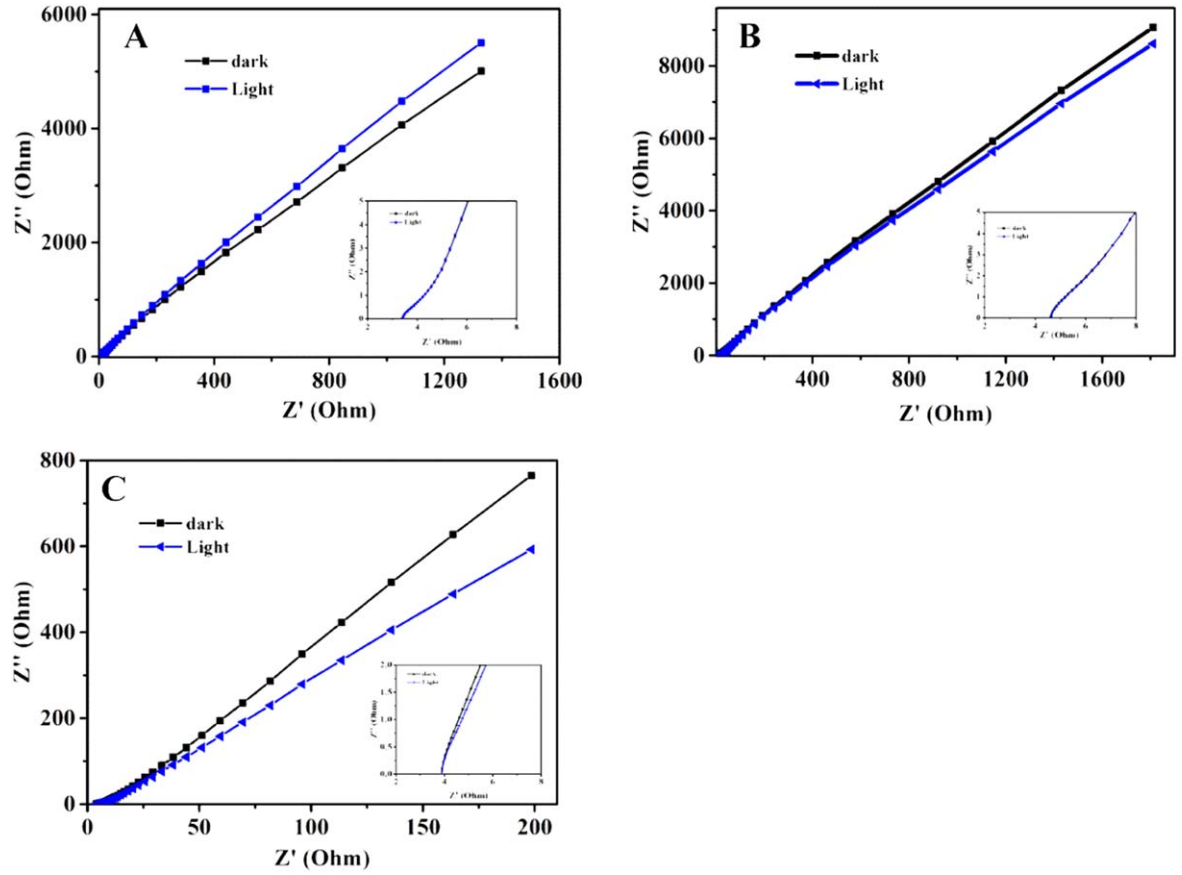

Figure 16. The impedance spectra of (A) as prepared (B) with annealing 200 °C (C) 300 °C Ag/ZnO/FTO thin film.

Figures 16(A)–(C) present the Nyquist plots under dark and white light irradiation of the as-prepared Ag/ZnO and those annealed at 200 °C and 300 °C, respectively. The spectra shows an intercept at a high frequency for the resistance of the electrolyte R_e on the intersection with the real axis Z', followed by the high-to-middle frequency range and the low frequency range to 0.1 Hz, which indicated an inclined line. The impedance spectrum is likely to be shaped like a semi-infinite Warburg [48]. The inclined line may be attributed to the diffusion of the ions into the electrode material in the process called the Warburg diffusion [49]. The figure shows that the photoanode has a clear response under light.

The values of the R_e parameter of the EIS spectra for the as prepared Ag/ZnO thin films under dark and light conditions are 3.437 and 3.395 Ω, respectively, while Ag/ZnO annealed at 200 °C under dark and light are 4.632 and 4.491 Ω, respectively. In state annealed at 300 °C under dark and light are 3.908 and 3.934 Ω.

4. Conclusions

The prepared Ag/ZnO nanorods core/shell samples appeared high photocatalytic activity for MB dye under low intensity of white light. High photocatalytic efficiency was observed for the sample annealed at 200 °C where degradation rate reached to 100% at short irradiation time of 90 min. The reason of the high degradation rate is surface area of prepared samples and great number of active surface sites at incident visible light on the Ag surface. Consequently, the photocatalysis process involved in a redox reaction such that the content of electrons, peroxide oxygen, and hydroxyl rote as strong oxidation were to lead interact with the pollution making it an effective photocatalyst. In the LSV measurement (J–V), the photocurrent density under light irradiation exceeded that under dark conditions, and response slightly photoanode deference between dark and photon light. The CV experiment under dark conditions was repeated six times using different scan rates of two cycles. Ag/ZnO nanorods core/shell electrodes exhibited nonfaradaic and pseudocapacitance behavior. Mott–Schottky measurements were performed for all photoanodes prepared under 100, 1000, and 10 000 Hz. Through these measurements, we observed the flat band potentials V_{FB} of all photoanodes of Ag/ZnO. The negative flat band potential fulfilled the Nernst equation and indicated the good performance of the photoanode electrode in the easy charge separation of photogenerated charge carriers and improvement of water splitting. The donor density value of the photoanode Ag/ZnO nanorod core/shell at 100 Hz was greater than that at 1000 and 10 000 Hz. Hence, the preferred frequency is 10 000 Hz, at which point the so-called metallization phenomenon occurs. Metallization leads to a decrease in the width of the space charge region where the field drop exists, consequently lowering the photocurrent density.

Data availability statement

No new data were created or analysed in this study.

ORCID iDs

M J Kadhim https://orcid.org/0000-0002-4985-9380
M A Mahdi https://orcid.org/0000-0002-9377-144X
J J Hassan https://orcid.org/0000-0003-4296-8450

References

[1] Lin D, Wu H, Zhang R and Pan W 2009 Enhanced photocatalysis of electrospun Ag–ZnO heterostructured nanofibers *Chem. Mater.* **21** 3479–84
[2] Hassan J J, Mahdi M A, Ramizy A, Hassan H A and Hassan Z 2013 Fabrication and characterization of ZnO nanorods/p-6H–SiC heterojunction LED by microwave-assisted chemical bath deposition *Superlattices Microstruct.* **53** 31–8
[3] Hassan J J, Mahdi M A, Chin C W, Abu-Hassan H and Hassan Z 2012 Room-temperature hydrogen gas sensor with ZnO nanorod arrays grown on a quartz substrate *Physica* E **46** 254–8
[4] Hassan J J, Mahdi M A, Chin C W, Abu-Hassan H and Hassan Z 2013 Room temperature hydrogen gas sensor based on ZnO nanorod arrays grown on a SiO_2/Si substrate via a microwave-assisted chemical solution method *J. Alloys Compd.* **546** 107–11
[5] Hassan J J, Hassan Z and Abu-Hassan H 2011 High-quality vertically aligned ZnO nanorods synthesized by microwave-assisted CBD with ZnO–PVA complex seed layer on Si substrates *J. Alloys Compd.* **509** 6711–9
[6] Georgekutty R, Seery M K and Pillai S C 2008 A highly efficient Ag–ZnO photocatalyst: synthesis, properties, and mechanism *J. Phys. Chem.* C **112** 13563–70
[7] Hu A, Zhang X, Oakes K D, Peng P, Zhou Y N and Servos M R 2011 Hydrothermal growth of free standing TiO_2 nanowire membranes for photocatalytic degradation of pharmaceuticals *J. Hazard. Mater.* **189** 278–85
[8] Hu A, Liang R, Zhang X, Kurdi S, Luong D, Huang H, Peng P, Marzbanrad E, Oakes K D and Zhou M R 2013 Enhanced photocatalytic degradation of dyes by TiO_2 nanobelts with hierarchical structures *J. Photochem. Photobiol.* A **256** 7–15
[9] Liang R, Hu A, Li W and Zhou Y N 2013 Enhanced degradation of persistent pharmaceuticals found in wastewater treatment effluents using TiO_2 nanobelt photocatalysts *J. Nanopart. Res.* **15** 10
[10] Lin C-Y, Lai Y-H, Balamurugan A, Vittal R, Lin C-W and Ho K-C 2010 Electrode modified with a composite film of ZnO nanorods and Ag nanoparticles as a sensor for hydrogen peroxide *Talanta* **82** 340–7
[11] Bai H, Liu Z and Sun D D 2011 Hierarchical ZnO/Cu 'corn-like' materials with high photodegradation and antibacterial capability under visible light *Phys. Chem. Chem. Phys.* **13** 6205–10
[12] Wu J-J and Tseng C-H 2006 Photocatalytic properties of nc-Au/ZnO nanorod composites *Appl. Catal.* B **66** 51–7
[13] Sinha G, Depero L E and Alessandri I 2011 Recyclable SERS substrates based on Au-coated ZnO nanorods *ACS Appl. Mater. Interfaces* **3** 2557–63
[14] Ren C, Yang B, Wu M, Xu J, Fu Z, Guo T, Zhao Y and Zhu C 2010 Synthesis of Ag/ZnO nanorods array with enhanced photocatalytic performance *J. Hazard. Mater.* **182** 123–9
[15] Wang H, Liu X, Wang S and Li L 2018 Dual templating fabrication of hierarchical porous three-dimensional ZnO/carbon nanocomposites for enhanced photocatalytic and photoelectrochemical activity *Appl. Catal.* B **222** 209–18
[16] Wu J, Du Y, Wang C, Bai S, Zhang T, Chen T and Hu A 2019 Reusable and long-life 3D Ag nanoparticles coated Si nanowire array as sensitive SERS substrate *Appl. Surf. Sci.* **494** 583–90
[17] Chouhan N, Liu R-S and Zhang J 2017 *Photochemical Water Splitting: Materials and Applications* (Boca Raton, FL, London: CRC Press, Taylor and Francis)
[18] Gao P, Ng K and Sun D D 2013 Sulfonated graphene oxide-ZnO–Ag photocatalyst for fast photodegradation and disinfection under visible light *J. Hazard. Mater.* **262** 826–35
[19] Shi X, Ma D, Ma Y and Hu A 2017 N-doping Ta_2O_5 nanoflowers with strong adsorption and visible light *J. Photochem. Photobiol.* A **332** 487–96
[20] Kadhim M J, Mahdi M A and Hassan J J 2020 Influence of pH on the photocatalytic activity of ZnO nanorods *Mater. Int.* **2** 0064–72
[21] Liang Y-C, Wang C-C, Kei C-C, Hsueh Y-C, Cho W-H and Perng T-P 2011 Photocatalysis of Ag-loaded TiO_2 nanotube arrays formed by atomic layer deposition *J. Phys. Chem.* C **115** 9498–502
[22] Kumar A and Pandey G 2017 A review on the factors affecting the photocatalytic degradation of hazardous materials *Mater. Sci. Eng. Int. J.* **1** 106–14
[23] Qiu Y, Yan K, Deng H and Yang S 2012 Secondary branching and nitrogen doping of ZnO nanotetrapods: building a highly active network for photoelectrochemical water splitting *Nano Lett.* **12** 407–13
[24] Zhang W-D, Jiang L-C and Ye J-S 2009 Photoelectrochemical study on charge transfer properties of ZnO nanowires promoted by carbon nanotubes *J. Phys. Chem.* C **113** 16247–53
[25] Sahoo P, Sharma A, Padhan S, Udayabhanu G and Thangavel R 2019 UV-assisted water splitting of stable Cl-doped ZnO nanorod photoanodes grown via facile sol–gel hydrothermal technique for enhanced solar energy harvesting applications *Sol. Energy* **193** 148–63
[26] Rasouli F, Rouhollahi A and Ghahramanifard F 2019 Gradient doping of copper in ZnO nanorod photoanode by electrodeposition for enhanced charge separation in photoelectrochemical water splitting *Superlattices Microstruct.* **125** 177–89
[27] Karmakar K, Sarkar A, Mandal K and Khan G G 2016 Stable and enhanced visible-light water electrolysis using C, N, and S surface functionalized ZnO nanorod photoanodes: engineering the absorption and electronic structure *ACS Sustain. Chem. Eng.* **4** 5693–702
[28] Pourshaban E, Abdizadeh H and Golobostanfard M R 2015 ZnO nanorods array synthesized by chemical bath deposition: effect of seed layer sol concentration *Proc. Mater. Sci.* **11** 352–8
[29] Abdallah B, Jazmatia A K and Refaaia R 2017 Oxygen effect on structural and optical properties of ZnO thin films deposited by RF magnetron sputtering *Mater. Res.* **20** 607–12
[30] Tarwal N L and Patil P S 2011 Enhanced photoelectrochemical performance of Ag–ZnO thin films synthesized by spray pyrolysis technique *Electrochim. Acta* **56** 6510–6
[31] Sabbaghan M, Firooz A A and Ahmadi V J 2012 The effect of template on morphology, optical and photocatalytic properties of ZnO nanostructures *J. Mol. Liq.* **175** 135–40
[32] Reuterglrdh L B and Langphasuk M 1997 Photocatalytic decolourization of reactive AZO dye: a comparison between TiO_2 and CdS photocatalysis *Chemosphere* **35** 585–96
[33] Saravanan R, Thirumal E, Gupta V K, Narayanan V and Stephen A 2013 The photocatalytic activity of ZnO prepared by simple thermal decomposition method at various temperatures *J. Mol. Liq.* **177** 394–401

[34] Whang T-J, Hsieh M-T and Chen H-H 2012 Visible-light photocatalytic degradation of methylene blue with laser-induced Ag/ZnO nanoparticles *Appl. Surf. Sci.* **258** 2796–801

[35] Saoud K, Alsoubaihi R, Bensalah N, Bora T, Bertino M and Dutta J 2015 Synthesis of supported silver nano-spheres on zinc oxide nanorods for visible light photocatalytic applications *Mater. Res. Bull.* **63** 134–40

[36] Sen T K, Afroze S and Ang H M 2011 Equilibrium, kinetics and mechanism of removal of methylene blue from aqueous solution by adsorption onto pine cone biomass of Pinus radiata *Water Air Soil Pollut.* **218** 499–515

[37] Sreedhar A, Reddy I N, Ta Q T H, Namgung G, Cho E and Noh J-S 2019 Facile growth of novel morphology correlated Ag/Co-doped ZnO nanowire/flake-like composites for superior photoelectrochemical water splitting activity *Ceram. Int.* **45** 6985–93

[38] Wei Y, Ke L, Kong J, Liu H, Jiao Z, Lu X, Du H and Sun X W 2012 Enhanced photoelectrochemical water-splitting effect with a bent ZnO nanorod photoanode decorated with Ag nanoparticles *Nanotechnology* **23** 235401

[39] Al-Asadi A S *et al* 2017 Aligned carbon nanotube/zinc oxide nanowire hybrids as high performance electrodes for supercapacitor applications *J. Appl. Phys.* **121** 124303

[40] Qi H, Bo Z, Yang S, Duan L, Yang H, Yan J, Cen K and Ostrikov K 2019 Hierarchical nanocarbon-MnO_2 electrodes for enhanced electrochemical capacitor performance *Energy Storage Mater.* **16** 607–18

[41] Deshmukh P R, Sohn Y and Shin W G 2017 Chemical synthesis of ZnO nanorods: Investigations of electrochemical performance and photo-electrochemical water splitting applications *J. Alloys Compd.* **711** 573–80

[42] Ramírez-Ortega D, Meléndez A M, Acevedo-Peña P, González I and Arroyo R 2014 Semiconducting properties of ZnO/TiO_2 composites by electrochemical measurements and their relationship with photocatalytic activity *Electrochim. Acta* **140** 541–9

[43] Rasouli F, Rouhollahi A and Ghahramanifard F 2019 Fabrication of silver nanoparticles decorated zinc oxide nanotubes by electrodeposition technique for photoelectrochemical water splitting *Mater. Sci. Semicond. Process.* **93** 371–8

[44] Akikusa J and Khan S U M 1997 Photoresponse and AC impedance characterization of n-TiO2 films during hydrogen and oxygen evolution reactions in an electrochemical cell *Int. J. Hydrog. Energy* **22** 875–82

[45] Li M, Yang Y, Yichuan L, Weitao Q, Fuxin W, Tianyu L, Yu S, Xiaoxia L, Pingping F and Yexiang T 2017 Morphology and doping engineering of Sn-doped hematite nanowire photoanodes *Nano Lett.* **17** 2490–5

[46] Nazarov A, Diler E, Persson D and Thierry D 2015 Electrochemical and corrosion properties of ZnO/Zn electrode in atmospheric environments *J. Electroanal. Chem.* **737** 129–40

[47] Asha K, Banerjee A, Saxena S, Khan S A, Sulaniya I, Satsangi V R, Shrivastav R, Kant R and Dass S 2019 Morphological influence of electrode/electrolyte interface towards augmenting the efficiency of photoelectrochemical water splitting—a case study on ZnO *J. Power Sources* **432** 38–47

[48] Nguyen T Q and Breitkopf C 2018 Determination of diffusion coefficients using impedance spectroscopy data *J. Electrochem. Soc.* **165** E826–31

[49] Cui Y, Zhao X and Guo R 2010 High rate electrochemical performances of nanosized ZnO and carbon co-coated $LiFePO_4$ cathode *Mater. Res. Bull.* **45** 844–9